JCTC Journal of Chemical Theory and Computation

New Variational Method for the Ab Initio Study in Valence Coordinates of the Renner−Teller Effect in Tetra-Atomic Systems

Laurent Jutier* and Céline Léonard

Université Paris-Est, Laboratoire Modélisation et Simulation Multi Echelle, MSME UMR 8208 CNRS, 5 bd Descartes, 77454 Marne-la-Vallée, France

Received February 5, 2010

Abstract: A new variational methodology for the treatment of the Renner−Teller effect in tetra-atomic molecules has been developed in valence coordinates. The kinetic-energy operator of Bramley et al. [*Mol. Phys.* **1991**, *73*, 1183] for any sequentially bonded four-atom molecule, A−B−C−D, in the singlet nondegenerate electronic state has been adapted to the Renner−Teller and spin couplings by modifying the expression of the nuclear angular momentum. The total Schrödinger equation is solved by diagonalizing the Hamiltonian matrix in a three-step contraction scheme. The main advantage of this new theoretical development is the possibility of studying different isotopomers using the same potential-energy surfaces. This procedure has been tested on $HCCH^+$ and its deuterated derivatives $DCCD^+$ and $DCCH^+$. The calculated rovibronic band origins were compared with previous data deduced from the Jacobi coordinates methodology, dimensionality reduced variational treatment, and photoelectron spectra with a good global agreement. Rotational structures for these systems are also tackled.

1. Introduction

The Renner−Teller effect is a key issue for the study of many linear radicals and ions. Indeed, only the infrared and microwave spectra obtained from Σ electronic states can be understood without taking into account the couplings between the rovibrational degrees of freedom and the electronic orbital momentum.

In a previous paper,[1] we described a new variational method for the treatment of the Renner−Teller effect in tetra-atomic systems using Jacobi coordinates. We included couplings between all degrees of freedom intervening in the molecular Hamiltonian: rotation, vibration, electronic orbital, and electronic spin. In this coordinate set, the central stretch links the centers of mass of both diatomic fragments. It was successfully applied on the low-energy rovibronic states of the acetylene cation.[2] Nevertheless, three points motivated the development of a new numerical method using valence coordinates. (i) For well-bounded systems, the valence coordinates often reduce the crossing terms in the potential-energy surfaces (PESs) compared to Jacobi coordinates. In the case of the acetylene cation, for which both external atoms are hydrogens, the difference between both coordinate sets is not crucial. On the other hand, for a system such as thioketenyl (HCCS), the center of mass of the CS fragment is closer to S than to C. This simple fact involves very high crossing terms between both central and CS stretches as well as with the angle between them. The PESs are then much more difficult to fit with an analytical function, and the basis set should be very flexible in the subspaces associated with highly coupled coordinates. (ii) In Jacobi coordinates, the definition of the central stretch is different from an isotopomer to another. It is then necessary to define new PESs for each one. On the other hand, in valence coordinates, it is possible to use exactly the same analytical form of the PESs for different isotopomers, such as $HCCH^+$, $DCCH^+$, and $DCCD^+$. (iii) In the previous contraction scheme, only the stretching part of the Hamiltonian was diagonalized in a first step while both bending modes, the rotation, and the electronic orbital and spin angular momenta were treated together directly from the primitive basis set. The high number of required basis functions constrained us to

* To whom correspondence should be addressed: E-mail: jutier@univ-mlv.fr.

10.1021/ct100071d
Published on Web 04/20/2010

converge the eigenstates without the spin angular momentum and to study its effects with less basis functions for the bending degrees of freedom. This procedure is closer to a perturbative scheme than to a variational one and was only valid because of the low value of the spin−orbit constant (about -30 cm^{-1}).

To achieve our goal, we start from the work of Bramley et al.,[3,4] who derived an exact form of the nuclear Hamiltonian for tetra-atomic systems. This form can be used for the study of the rovibrational spectra from Σ electronic states, for which its dependence with the total angular momentum and its projections on the body-fixed (BF) axes are not differentiated from the nuclear contributions. For Renner−Teller systems, it must then be modified by subtracting the effects of the electronic orbital and spin angular momenta, following the same principle used for triatomic systems.[5,6] Moreover, in the case of a nonzero value of the electronic orbital momentum, the electronic part of the Hamiltonian depends on the choice of the BF axes because of the form of nonadiabatic couplings terms (NACTs) due to the torsion.

The present methodology has been tested on the $X^2\Pi$ electronic ground states of $HCCH^+$ and its deuterated isotopomers $DCCH^+$ and $DCCD^+$. $HCCH^+$ has the advantage of being well-studied experimentally and theoretically. It represents hence a benchmark system to validate our previous theoretical treatment based on the use of Jacobi coordinates.[1,2] Indeed, recent photoelectron spectra have been recorded by Tang et al.[7] and Yang and Mo[8] with a high resolution of the rovibronic bands of $HCCH^+$. The $DCCH^+$ and $DCCD^+$ photoelectron spectra of Reutt et al. allowed us to obtain some information about the vibrational modes of the deuterated species.[9]

Using their reduced degrees of freedom variational treatment, Perić et al. studied also the Renner−Teller effect and the spin−orbit coupling in the electronic ground state $^2\Pi$ of $DCCH^+$[10] and $^2\Pi_u$ of the symmetric species $HCCH^+$, $DCCD^+$.[11,12] Their approach was based on a harmonic representation of the potential-energy surfaces using the Renner−Teller parameters. The nuclear kinetic-energy operator considers derivatives with respect to four polar coordinates which describe the trans and cis bending vibrations, torsion and rotation around the axis associated with the smallest moment of inertia. These works were the first theoretical treatment of the Renner−Teller effect in symmetric and asymmetric linear tetra-atomic molecules.

The importance of modeling the spectroscopy of isotopomer species with a minimum computational effort must be emphasized, since deuterated istopomers of $HCCH^+$ are present in interstellar medium in which the chemistry is dominated by reactions between neutral and ionic molecules.[13] Moreover, the fraction H/D in comets water indicates that this water could be synthesized in interstellar medium.[14]

This paper is structured as follows. The complete definition of the Bramley et al. molecular Hamiltonian is explained in section 2. The modifications of the nuclear kinetic-energy operator and the total Hamiltonian related to the treatment of the Renner−Teller and spin−orbit couplings are given in section 3 as well as the contraction scheme and the primitive basis sets for each degree of freedom. The present methodology was checked by comparing rovibrational energies of the $X^3\Sigma_g^-$ electronic ground state of $HCCH^{2+}$ obtained from the present code, without taking into account the electronic angular momenta (i.e., $\Lambda = 0$, $S = 0$), and a variational code based on work by Bramley et al. In the last section, we validate the code and the associated methodology by comparison of our final rovibronic states of $HCCH^+$ and its isotopomers with already existent results, given by theory[2,11,12] and experiments.[7−9] Information concerning the rotational structures of both deuterated isotopomers is predictive.

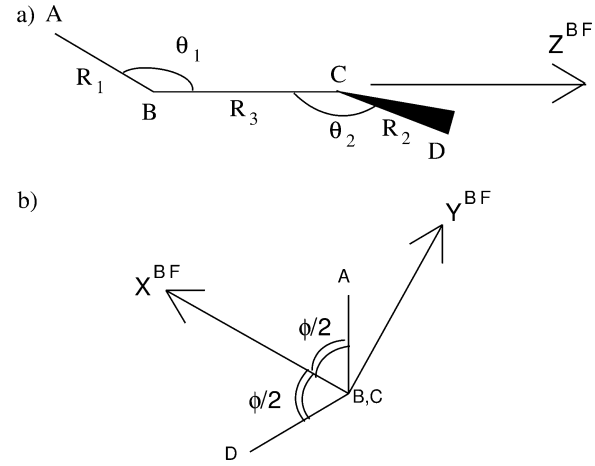

Figure 1. Definition of the valence coordinates and of the body-fixed (BF) frame.

2. Rovibrational Energies of a Nondegenerate Electronic State

This section summarizes the work done by Bramley et al.[3,4] that we used as the starting point for our new methodology. These authors determined an efficient variational method for calculating the rovibrational eigenstates of any sequentially bonded four-atom molecule, A−B−C−D. This method is suitable only for a singlet nondegenerate electronic state, since the nuclear kinetic-energy operator is a function of $\hat{\mathbf{J}}$, which refers to the total rovibrational angular momentum, i.e., neither orbital ($\hat{\mathbf{L}}$) nor spin ($\hat{\mathbf{S}}$) electronic angular momenta are considered, and the spin−orbit effects have not been introduced.

2.1. Rovibrational Hamiltonian. In the Born−Oppenheimer approximation, the molecular Hamiltonian can be decomposed as:

$$\hat{H}_{VR} = \hat{T}_{VR} + \hat{V}_N \tag{1}$$

The exact kinetic-energy operator $\hat{T}_{VR}$ is expressed in internal valence coordinates defined as follows. R_1, R_2, and R_3 are, respectively, the A−B, C−D, and B−C internuclear distances (Figure 1a). θ_1 and θ_2 are, respectively, the $\widehat{ABC}$ and $\widehat{BCD}$ angles (Figure 1a). Both vary in the interval $[0{:}\pi]$. ϕ is the dihedral angle between the planes defined by A, B, C and B, C, D (Figure 1b). This angle is in the $[0{:}2\pi]$ range. The origin O of the body-fixed frame is the center of mass of the whole system. The Z^{BF} axis is defined by the direction of the $\overrightarrow{BC}$ vector (Figure 1a). The B−C bond does not necessarily coincide with the Z^{BF} axis because of the

center of mass position. The X^{BF} axis is perpendicular to Z^{BF} and a bisector of the torsional dihedral angle ϕ (Figure 1b). The Y^{BF} axis is such that (O, X^{BF}, Y^{BF}, Z^{BF}) is a direct orthogonal frame (Figure 1b). The Euler angles (α, β, γ) link the space-fixed frame to the body-fixed frame defined above and are associated with the whole-molecule rotation angles. Derivatives with respect to these angles in $\hat{T}_{VR}$ are replaced by $\hat{J}_x$, $\hat{J}_y$, $\hat{J}_z$, where $\hat{\mathbf{J}}$ represents the rovibrational angular momentum about body-fixed axes through the nuclear center of mass, obeying anomalous commutation relations.[15,16]

The translation motion, which can be exactly decoupled from all other degrees of freedom, was removed from $\hat{T}_{VR}$ by placing the origin of the body-fixed frame at the molecular center of mass.

The use of valence internal coordinates is often very appropriate for a polynomial expansion form of $\hat{V}_N$ in the case of bonded systems, except for the torsion which must verify a modulo 2π periodicity. V_N is then modeled by a compact and factorizable expansion:

$$V_N = \sum_i C_i (R_1 - R_{1_{eq}})^{n_{1_i}} (R_2 - R_{2_{eq}})^{n_{2_i}} (R_3 - R_{3_{eq}})^{n_{3_i}} \times (\theta_1 - \pi)^{n_{4_i}} (\theta_2 - \pi)^{n_{5_i}} \cos(n_{6_i}\phi) \quad (2)$$

In these coordinates $\hat{T}_{VR}$ is also separable and factorizable. The complete form can be found in the annexes of refs 3 and 4.

2.2. Primitive Basis Functions. The complexity of $\hat{T}_{VR}$ is compensated by the cheap evaluation of the Hamiltonian matrix elements calculated from products of one-dimensional integrals.

Before any contraction achieved by the resolution of the Schrödinger equation in a given subspace, the primitive basis functions can be expressed in the general form

$$\Phi_{\text{rovib}} = \Phi_i^{str3D}(R_1, R_2, R_3) \cdot P_{l_1}^{m_1}(\theta_1) \cdot P_{l_2}^{m_2}(\theta_2) \cdot e^{i\omega\phi} \cdot |J, K, M\rangle \quad (3)$$

where $|J,K,M\rangle$ is a rotational symmetric top function in which K is the eigenvalue of $\hat{J}_z$ in the body-fixed frame (BF) and M in the space-fixed frame (SF). In the absence of external electric fields, the quantum number M can be dropped.

The rules

$$\left.\begin{array}{ll} K(\text{odd}) & \Rightarrow \ \omega = (2m+1)/2 \\ K(\text{even}) & \Rightarrow \ \omega = m \end{array}\right\} m = 0, 1, 2, \ldots \quad (4)$$

impose that Φ_{rovib} is single valued for ϕ and γ moving in the range $0 \rightarrow 2\pi$.

$P_{l_i}^{m_i}$ functions remove singularities of $\hat{T}_{VR}$ if

$$\begin{aligned} &\text{for } m_1 = 0, \quad \omega = \frac{K}{2} \\ &\text{for } m_2 = 0, \quad \omega = -\frac{K}{2} \end{aligned} \quad (5)$$

Basis functions that violate these rules have infinite expectation values across $\hat{T}_{VR}$.

The stretch basis set, $\Phi^{str3D}(R_1, R_2, R_3)$, is made by the 1-dimensional products of harmonic or Morse oscillators of q_1, q_2, R_3 coordinates, $\Phi_{v_1}(q_1)\Phi_{v_2}(q_2)\Phi_{v_3}(R_3)$. q_1, q_2 are the symmetrized combinations of R_1, R_2 in the case of the $D_{\infty h}(M)$ system or equal to R_1, R_2 otherwise.

3. Rovibronic Energies of a Degenerate Electronic State

For linear degenerate electronic states, the couplings between orbital, spin electronic, and rovibrational angular momenta should be taken into account.

3.1. Rovibronic Hamiltonian. The Hamiltonian that considers the Renner−Teller and spin−orbit effects is

$$\hat{H} = \hat{T}_N + \hat{H}_e + \hat{H}_{SO} \quad (6)$$

where $\hat{H}_e$ is the electronic Hamiltonian and $\hat{H}_{SO}$ is the perturbative spin−orbit contribution. $\hat{T}_N$ comes from the adapted kinetic-energy operator $\hat{T}_{VR}$ in the valence coordinates of Bramley et al.[3,4] described in the previous section to the Renner−Teller and spin−orbit treatment.

In molecules having a nonzero electronic angular momentum, either orbital ($\hat{\mathbf{L}}$) or spin ($\hat{\mathbf{S}}$) or both, $\hat{\mathbf{J}}$ refers to the total rovibronic angular momentum and the $\hat{\mathbf{J}}$ introduced in section 2.1 must be replaced by $\hat{\mathbf{J}}-\hat{\mathbf{L}}-\hat{\mathbf{S}}$ in $\hat{T}_N$. Indeed, the kinetic-energy operator depends only on nuclear coordinates. The projections of the total angular momentum on the BF axes $\hat{J}_{x,y,z}$ are replaced by $\hat{J}_{x,y,z}-\hat{S}_{x,y,z}-\hat{L}_{x,y,z}$, $\hat{S}_{x,y,z}$ and $\hat{L}_{x,y,z}$ being the projections of the electron spin and orbital angular momenta on the BF axes, respectively. Focusing on a single degenerate electronic state well isolated from all other ones, it is possible to neglect the effects of both $\hat{L}_x$ and $\hat{L}_y$ projections of the electronic orbital momentum on the X^{BF} and Y^{BF} axes. $\hat{J}_{x,y,z}$ obeys anomalous commutation rules,[16−18] whereas $\hat{L}_{x,y,z}$ and $\hat{S}_{x,y,z}$ obey normal ones:

normal commutation rules:

$$\begin{aligned} \hat{S}_x|S,\Sigma\rangle &= \frac{1}{2}\sqrt{S(S+1) - \Sigma(\Sigma+1)}|S,\Sigma+1\rangle \\ &\quad + \frac{1}{2}\sqrt{S(S+1) - \Sigma(\Sigma-1)}|S,\Sigma-1\rangle \\ \hat{S}_y|S,\Sigma\rangle &= \frac{-i}{2}\sqrt{S(S+1) - \Sigma(\Sigma+1)}|S,\Sigma+1\rangle \\ &\quad + \frac{i}{2}\sqrt{S(S+1) - \Sigma(\Sigma-1)}|S,\Sigma-1\rangle \end{aligned} \quad (7a)$$

anomalous commutation rules:

$$\begin{aligned} \hat{J}_x|J,P\rangle &= \frac{-i}{2}\sqrt{J(J+1) - P(P+1)}|J,P+1\rangle \\ &\quad + \frac{i}{2}\sqrt{J(J+1) - P(P-1)}|J,P-1\rangle \\ \hat{J}_y|J,P\rangle &= \frac{1}{2}\sqrt{J(J+1) - P(P+1)}|J,P+1\rangle \\ &\quad + \frac{1}{2}\sqrt{J(J+1) - P(P-1)}|J,P-1\rangle \end{aligned} \quad (7b)$$

where $|S,\Sigma\rangle$ and $|J,P\rangle$ are the eigenstates of $\hat{S}_z$, $\hat{S}^2$ and $\hat{J}_z$, $\hat{J}^2$, respectively, such as the quantum numbers Σ and P are defined by $\hat{S}_z|S,\Sigma\rangle = \Sigma|S,\Sigma\rangle$ and $\hat{J}_z|J,P\rangle = P|J,P\rangle$ with

$$P = K + \Lambda + \Sigma \quad (8)$$

where K and Λ correspond to the quantum numbers associated with the projections on Z^{BF} of the rovibrational and electronic angular momenta, $\hat{\mathbf{J}}_N = \hat{\mathbf{J}}-\hat{\mathbf{L}}-\hat{\mathbf{S}}$ and $\hat{\mathbf{L}}$, respectively.

3.2. Electronic States. If, for bent geometries, each component of a degenerate electronic state correlates to a Π or Δ, Φ... electronic state at linearity, the eigenvectors $|\pm\Lambda\rangle$ of the electronic orbital angular momentum, $\hat{L}_z$, can still be used as a basis set for the electronic orbital part of the total rovibronic wave function. Then $\hat{L}_z|+\Lambda\rangle = +\Lambda|+\Lambda\rangle$ and $\hat{L}_z|-\Lambda\rangle = -\Lambda|-\Lambda\rangle$, where Λ is the absolute value of the projection of the electronic orbital momentum on Z^{BF}.

On the other hand, operators $\hat{L}_{x,y}$ only couple electronic states associated with values of Λ differing of ±1, for instance, a Σ electronic state close in energy to a Π electronic state. The action of these operators has been neglected.

The basis functions for the electronic orbital degree of freedom are then

$$\Phi_e^{\pm} = |\pm\Lambda\rangle \approx e^{\pm i\Lambda(\theta_e^{BF})} = \frac{X \pm iY}{\sqrt{2}} \tag{9}$$

X and *Y* correspond to the real electronic components of the considered degenerate electronic state.

$\hat{L}_z$ is defined as $-i(\partial)/(\partial\theta_e^{BF})$, where θ_e^{BF} is the collective electronic orbital angle. If the electronic state results from a configuration with only one electron or one vacuum in a degenerate molecular orbital, θ_e^{BF} is associated with this only unpaired electron or vacuum in the one-electron approximation. In the body-fixed frame defined in section 2.1, the electronic Hamiltonian, $\hat{H}_e$, expressed in the basis set $\{\Phi_e^+, \Phi_e^-\}$ is

$$\tilde{H}_e = \begin{pmatrix} \frac{V^X + V^Y}{2} & \frac{V^X - V^Y}{2} \\ \frac{V^X - V^Y}{2} & \frac{V^X + V^Y}{2} \end{pmatrix} \tag{10}$$

V^X and V^Y are the potential-energy surfaces associated with *X* and *Y* electronic states. It must be noted that the electronic Hamiltonian matrix $\tilde{H}_e$ differs from the one described in ref 1 due to a theoretical development in a body-fixed frame defined such that reference plane ($X^{BF}OZ^{BF}$) is the bisector of the dihedral angle ϕ (see Figure 1) instead of E_2 in ref 1. For the same reason, the nonadiabatic electronic coupling terms characteristic of the Renner−Teller effect are simply

$$\left\langle Y \left| \frac{\partial}{\partial\gamma} \right| X \right\rangle \simeq \Lambda; \quad \left\langle Y \left| \frac{\partial}{\partial\phi} \right| X \right\rangle \simeq 0 \tag{11}$$

Both frameworks are equivalent.

When the molecule is linear, both electronic components are degenerate and the potential-energy surface can be described by the following analytical function

$$V_{stretch} = \sum_{ijk} A_{ijk}(R_1 - R_{1,eq})^i(R_2 - R_{2,eq})^j(R_3 - R_{3,eq})^k \tag{12}$$

where $R_{i,eq}$ is the reference for the R_i stretch and $A_{ijk} = A_{jik}$ for symmetry reasons.

When the molecule is no longer linear, it is necessary to express two PESs. We directly fitted $(V^X + V^Y)/2 = V^{average}$ and $(V^X - V^Y)/2 = V^{diff}$ rather than V^X and V^Y. For pure bending displacements:

$$\begin{aligned} V_{bend}^{average} &= \sum_{lmn} B_{lmn} \cdot \theta_1^l \cdot \theta_2^m \cdot \cos(n\phi^{BF}) \\ V_{bend}^{diff} &= \sum_{lmn} C_{lmn} \cdot \theta_1^l \cdot \theta_2^m \cdot \cos(n\phi^{BF}) \end{aligned} \tag{13}$$

For couplings between bending and stretching displacements:

$$\begin{aligned} V_{sb}^{average} = \sum_{ijklmn} D_{ijklmn}(R_1 - R_{1,eq})^i(R_2 - R_{2,eq})^j \times \\ (R_3 - R_{3,eq})^k \cdot \theta_1^l \cdot \theta_2^m \cdot \cos(n\phi^{BF}) \\ V_{sb}^{diff} = \sum_{ijklmn} E_{ijklmn}(R_1 - R_{1,eq})^i(R_2 - R_{2,eq})^j \times \\ (R_3 - R_{3,eq})^k \theta_1^l \theta_2^m \cdot \cos(n\phi^{BF}) \end{aligned} \tag{14}$$

These expressions of the analytical PESs are similar to the ones used in our previous study.[1]

The potential energies were evaluated for 204 independent geometries in the C_S symmetry point group, i.e., $\phi^{BF} = 0$ (cis conformation) or $\phi^{BF} = \pi$ (trans conformation). *X*, *Y* are correlated to the *A*, *B* irreducible representations in the C_2 point group, respectively. The RCCSD(T) method[19−21] and the cc-pV5Z basis set[22] were used within the MOLPRO package.[23] The global rms is less than 0.5 cm^{-1}, with 35 independent coefficients for the average surface, $V^{average}$ and 18 for V^{diff} (which does not contain pure stretching coefficients). All coefficients of the analytical representations of the PESs are given.

Table 1 gives the coefficients for the pure stretching part of the average surface A_{ijk}.

Table 2 gives the coefficients for the pure bending part of the average surface B_{ijk}.

In Table 3 the coefficients for the couplings between bending and stretching modes of the average surface D_{ijklmn} are listed.

Table 1. Coefficients of the Analytic Representation of the Degenerate PES at Linearity, $V_{stretch}$ of Eq 12 (in au)[a]

A_i	n_1	n_2	n_3
−76.797258052	0	0	0
0.18775932871	2/0	0/2	0/0
0.00049219849978	1	1	0
−0.010446131479	1/0	0/1	1/1
0.44482987202	0	0	2
−0.18875621850	3/0	0/3	0/0
0.0034470302368	2/0	0/2	1/1
−0.00046558758339	1/0	0/1	2/2
−0.45136275104	0	0	3
0.12843527244	4/0	0/4	0/0
−0.0024256691021	3/0	0/3	1/1
−0.0042693423415	2/0	0/2	2/2
0.29119003380	0	0	4
−0.15477459177	0	0	5
0.058833359015	0	0	6
−0.080493877749	5/0	0/5	0/0
−0.0022746306025	3/2	2/3	0/0
0.041225800651	6/0	0/6	0/0

[a] When $n_1 \neq n_2$, the A_i coefficients are common to triplets in which n_1 and n_2 are inverted. The zeroth-order coefficient, involving only a global shift for the wavefunction energies, is not considered in variational calculations. $R_{1,eq}$, $R_{2,eq}$, and $R_{3,eq}$ are defined such that the first-order coefficients cancel: $R_{1,eq} = R_{2,eq} = 2.0382$ bohr and $R_{3,eq} = 2.3627$ bohr.

Table 2. Coefficients of the Analytic Representation of the Average PES, $V_{bend}^{average}$ of Eq 13 (in au)[a]

B_i	n_1	n_2	n_3
0.031380342315	2/0	0/2	0/0
−0.00010589082066	4/0	0/4	0/0
0.0075651209859	2	2	0
−0.00032900039217	6/0	0/6	0/0
0.015301967243	1	1	1
−0.0069697677988	3/1	1/3	1/1
0.0052863195870	3	3	1

[a] When $n_4 \neq n_5$, the B_i coefficients are common to triplets in which n_4 and n_5 are inverted.

Table 3. Coefficients of the Analytic Representation of the Average PES, $V_{sb}^{average}$ of Eq 14 (in au)[a]

D_i	n_1	n_2	n_3	n_4	n_5	n_6
−0.0085356746578	1/0	0/1	0/0	2/0	0/2	0/0
−0.0016760742892	1/0	0/1	0/0	1/1	1/1	1/1
−0.0017279408242	0/1	1/0	0/0	2/0	0/2	0/0
−0.036304901251	0/0	0/0	1/1	2/0	0/2	0/0
0.028175216677	0	0	1	1	1	1
−0.0015969509525	2/0	0/2	0/0	2/0	0/2	0/0
−0.0014800493600	2/0	0/2	0/0	1/1	1/1	1/1
−0.0082527829467	0/0	0/0	2/2	2/0	0/2	0/0
0.0050003688608	0	0	2	1	1	1
0.011960852836	1/0	0/1	1/1	2/0	0/2	0/0

[a] When $(n_1, n_4) \neq (n_2, n_5)$, the D_i coefficients are common to sextuplets in which (n_1, n_4) and (n_2, n_5) are inverted.

Table 4. Coefficients of the Analytic Representation of the Difference PES, V_{bend}^{diff} of Eq 13 (in au)[a]

C_i	n_1	n_2	n_3
−0.0040713277155	2	2	0
−0.023659941406	4/2	2/4	0/0
−0.00024053133094	5/1	1/5	1/1
0.0062884157463	2/0	0/2	1/1
−0.0040251186102	4/0	0/4	1/1
0.0075451909845	2	2	1
−0.00037799117499	6/0	0/6	1/1
−0.015284625238	1	1	0
0.055519559631	3	3	0

[a] When $n_4 \neq n_5$, the C_i coefficients are common to triplets in which n_4 and n_5 are inverted.

Table 5. Coefficients of the Analytic Representation of the Difference PES, V_{sb}^{diff} of Eq 14 (in au)[a]

E_i	n_1	n_2	n_3	n_4	n_5	n_6
−0.0016889980478	1/0	0/1	0/0	2/0	0/2	1/1
−0.00085785320357	1/0	0/1	1/1	1/1	1/1	0/0
0.00020147090259	0/1	1/0	0/0	2/0	0/2	1/1
0.029003257627	0/0	0/0	1/1	2/0	0/2	1/1
−0.0058076857757	0	0	1	1	1	0
−0.0014955409812	2/0	0/2	0/0	2/0	0/2	1/1
0.00059036218845	0/2	2/0	0/0	2/0	0/2	1/1
−0.013421739988	0/0	0/0	2/2	2/0	0/2	1/1
−0.0015540891813	1/0	0/1	1/1	2/0	0/2	1/1

[a] When $(n_1, n_4) \neq (n_2, n_5)$, the E_i coefficients are common to sextuplets in which (n_1, n_4) and (n_2, n_5) are inverted.

Table 4 lists the coefficients for the pure bending degrees of freedom part of the difference surface C_{lmn}.

Table 5 lists the coefficients for the couplings between bending and stretching degrees of freedom of the difference surface E_{ijklmn}.

The polynomial expansion is used in the area of the configuration space in which ab initio points were computed, corresponding to the energy range of our present study. This range must at least correspond to the sum of the global zero-point energy (ZPE), the maximum of the excitation energy, and a margin due to a tunneling effect. However, the only way of verifying the energy range is to plot the final wave functions, which have to be well localized in the range of ab initio points. We chose the range $[\pi{:}1.92]$, appearing (more than) sufficient regarding the shapes of stationary states up to $\simeq$1800 cm^{-1} from the ZPE.

Figures 2 and 3 show that the average PES has a standard shape. The harmonic terms are predominant for θ_1 or θ_2 less than 60° from linearity. Non-negligible crossing terms are present between the bending and the central stretching modes in the trans conformation (see Figure 3).

The behavior of the difference PES is less intuitive and differs strongly from cis to trans conformations, as shown in Figure 4. In the trans conformation, both electronic components, V^X and V^Y, are well separated. The A' one (correlates to B in the C_2 symmetry point group) lies higher in energy than the A'' one (correlates to A in C_2). In the cis conformation, V^X and V^Y are almost degenerate, especially if $\theta_1 = \theta_2$, as already noted in our previous papers.[1,2]

The PES shapes are slightly different from Jacobi to valence coordinates, but the same conclusions remain. The definition of Renner−Teller parameters is not recommended since the perturbative approach, derived from the harmonic approximation, is unable to describe the near degeneracy of both electronic components in the cis conformation. As in previous works,[1,2] the conical intersection is reproduced by connecting parts of the PESs in the cis and trans conformations associated with the same irreducible representation A or B in the C_2 symmetry point group. Explicit ab initio computations of electronic energies in the C_1 symmetry point group would require a diabatization process, which is here achieved by smoothing the curves at the vicinity of conical intersections.

3.3. Basis Functions and Contraction Scheme. The primitive basis set is composed by products of one-dimensional functions, one by degree of freedom in the assumption that a factorizable and partially separable Hamiltonian is used:

$$\Phi_{prim}^{rovib} = \Phi_{v_1}(R_1)\Phi_{v_2}(R_2)\Phi_{v_3}(R_3)\cdot P_{l_1}^{m_1}(\theta_1)\cdot P_{l_2}^{m_2}(\theta_2)\cdot e^{i\omega\phi}\cdot |J,P\rangle\cdot \Phi_e^{\pm}\cdot |S,\Sigma\rangle \quad (15)$$

The diagonalization of the complete molecular Hamiltonian (eq 6) directly from this primitive basis set is by far too expensive in terms of memory and CPU time. A successive step contraction scheme is then settled starting with the diagonalization of subspaces using parts of $\hat{H}$. In the present study of the acetylene cation and its isotopomers, the following procedure was achieved. (1) $\Psi_{v_i}^{str3D}(R_1, R_2, R_3)$ contracted functions are first optimized in the 3-dimensional space associated with the stretches, $\{R_1, R_2, R_3\}$. (2) For *each* stretching contraction $\Psi_{v_i}^{str3D}(R_1, R_2, R_3)$, vibronic origins of bands are obtained

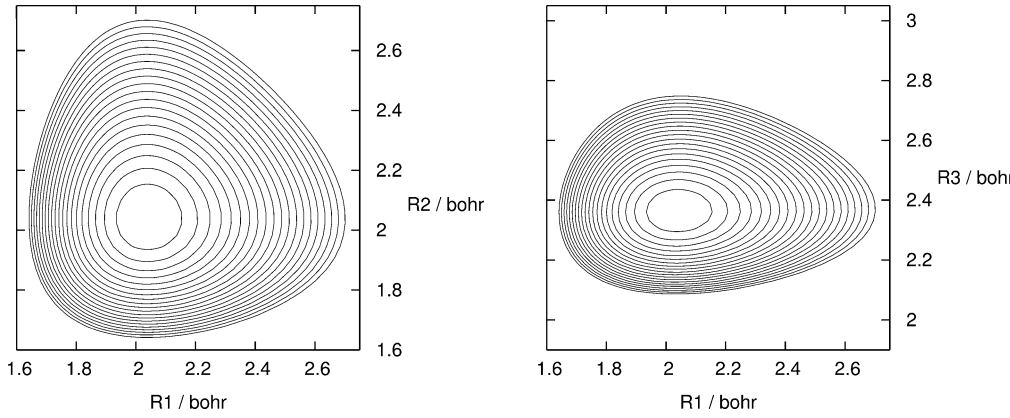

Figure 2. Two-dimensional contour plots of the average potential at linearity. The nonvarying bond length is fixed at its equilibrium geometry ($R_3 = 2.3627$ bohr and $R_2 = 2.0382$ bohr). The isolevel spacing is 500 cm^{-1}.

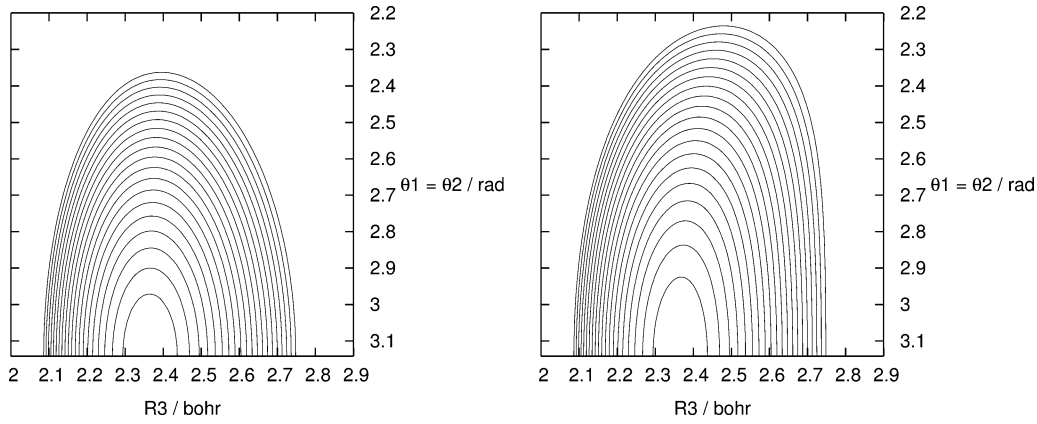

Figure 3. Two-dimensional contour plots of the average potential for R_1 and R_2 fixed at their equilibrium values. On the left-hand side, the torsion is fixed at 0 (cis conformation). On the right-hand side, the torsion is fixed at π (trans conformation). The isolevel spacing is 500 cm^{-1}.

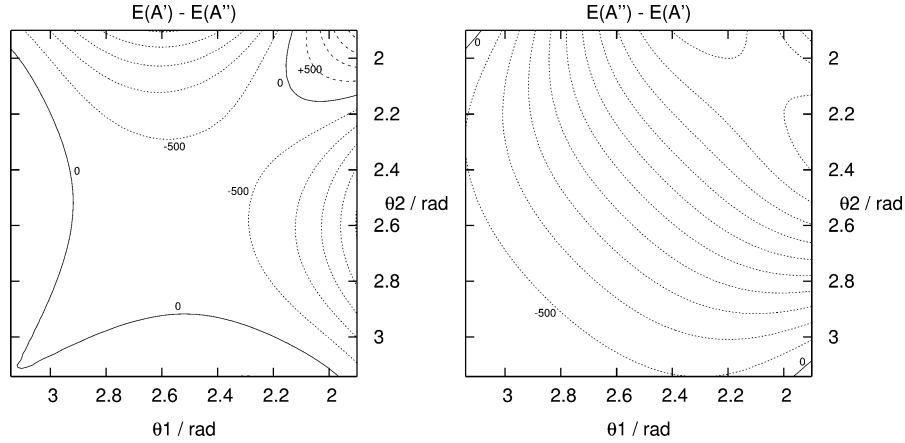

Figure 4. Two-dimensional contour plots of the difference potential for R_1, R_2, and R_3 fixed at their equilibrium values. On the left-hand side, the torsion is fixed at 0 (cis conformation). On the right-hand side, the torsion is fixed at π (trans conformation). Angles are in radians. The isolevel spacing is 500 cm^{-1}.

considering the four angles space, $\{\theta_1, \theta_2, \phi, \gamma\}$: $\Phi^{\text{vib}}_{vi,bi,P,\Lambda,\Sigma} = \Psi^{\text{str3D}}_{v_i}(R_1, R_2, R_3) \cdot \Psi^{\text{bend3D}}_{b_i}(\theta_1, \theta_2, \phi) \cdot e^{i(P-\Lambda-\Sigma)\gamma}$. For these functions, the P and Σ quantum numbers are considered as good quantum numbers. Then each triplet (v_i, P, Σ) corresponds to independent calculations. (3) All previous contractions are collected together and coupled by the complete molecular Hamiltonian $\hat{H}$. The only good quantum number is J, associated with the total angular momentum.

While the only observable is the complete Hamiltonian $\hat{H}$, the physical meaning of subspaces as well as convergence criteria is not trivial. Different contraction schemes can be convenient depending on the stronger coupling terms in the PESs (see discussion in ref 4).

The following parts detail the different steps of this contraction scheme.

3.3.1. Stretching States. The first step of the contraction scheme is the diagonalization of the pure stretching Hamil-

tonian $\hat{H}_{\text{stretch}}$. The considered molecular geometries are linear ($\theta_1 = \theta_2 = \pi$ and ϕ is not defined). The reduced Hamiltonian is

$$\hat{H}_{\text{stretch}} = -\frac{1}{2}\left[\frac{1}{\mu_1}\frac{\partial^2}{\partial R_1^2} + \frac{1}{\mu_2}\frac{\partial^2}{\partial R_2^2} + \frac{1}{\mu_3}\frac{\partial^2}{\partial R_3^2}\right] \quad (16a)$$

$$+ \cos(\theta_1)\left[\frac{-1}{m_B R_1 R_3} - \frac{1}{m_B}\frac{\partial^2}{\partial R_1 \partial R_3}\right] \quad (16b)$$

$$+ \cos(\theta_2)\left[\frac{-1}{m_C R_2 R_3} - \frac{1}{m_C}\frac{\partial^2}{\partial R_2 \partial R_3}\right] \quad (16c)$$

$$+ V_{\text{stretch}} \quad (16d)$$

with

$$\mu_1 = m_A m_B/(m_A + m_B)$$
$$\mu_2 = m_C m_D/(m_C + m_D)$$
$$\mu_3 = m_B m_C/(m_B + m_C) \quad (17)$$

The relation (eq 16a) is very similar to the stretching part of the nuclear kinetic-energy operator in Jacobi coordinates[1] but with a different definition of R_3. In valence coordinates, R_3 is the B−C internuclear bond length while R_3 is the distance between both centers of mass of diatomic fragments A−B and C−D in Jacobi coordinates. Thus, the terms in eqs 16b and 16c are absent in $\hat{T}_N$ expressed in Jacobi coordinates. They are not simple couplings between the different valence stretches since they involve additionally the bending angles θ_1 and θ_2 by way of their cosines. For linear configurations, these cosines are fixed at −1, and as a consequence, the pure stretching vibrational energies become slightly overestimated by $\lesssim$2%. This issue will be raised in the following steps of the contraction scheme.

For the variational calculations, basis functions are products of three eigenfunctions of the harmonic oscillator

$$\Phi^{\text{str3D}}_{v_1,v_2,v_3}(R_1, R_2, R_3) = \Phi^{\alpha_1}_{v_1}(R_1 - R_{1,\text{eq}}) \cdot \Phi^{\alpha_2}_{v_2}(R_2 - R_{2,\text{eq}}) \cdot \Phi^{\alpha_3}_{v_3}(R_3 - R_{3,\text{eq}}) \quad (18)$$

where

$$\Phi^{\alpha}_{v}(X) = \frac{1}{\sqrt{2^v v!}}\left(\frac{\alpha}{\pi}\right)^{1/4} H_v(\sqrt{\alpha}X)\mathrm{e}^{-\alpha X^2/2} \quad (19)$$

H_v is the Hermite polynomial of order v, and α is linked to the force constant and to the reduced mass associated to a given one-dimensional binding potential

$$\alpha_i = \sqrt{k_i \mu_i} \text{ with } k_1 = k_2 = 3.775 \text{ au and } k_3 = 0.8897 \text{ au} \quad (20)$$

Only the values of the reduced masses are modified when different isotopomers are considered.

The diagonalization of $\hat{H}_{\text{stretch}}$ gives optimized three-dimensional stretching contractions

$$\Psi^{\text{str3D}}_i(R_1, R_2, R_3) = \sum_j C^i_j \Phi^{\text{str3D}}_{v_{1_j},v_{2_j},v_{3_j}}(R_1, R_2, R_3) \quad (21)$$

The convergence of the stretching vibrational energies is reached for $HCCH^+$, $DCCH^+$, and $DCCD^+$ with $v_{1_{\max}} = v_{2_{\max}} = 10$ and $v_{3_{\max}} = 15$ leading to 559 basis functions $\Phi^{\text{str3D}}_{v_1,v_2,v_3}$, the grid of ($v_1$, v_2, v_3) values being nonrectangular. The convergence of vibrational states associated with the central stretch R_3 requires more basis functions than the external stretches due to stronger anharmonicity.

3.3.2. Vibronic States. In the second step of the contraction scheme, all vibrational terms of the kinetic-energy operator $\hat{T}_N$ are used, including those depending on $\hat{J}_z$ after the following transformation

$$\hat{J}_z \rightarrow \hat{J}_z - \hat{L}_z - \hat{S}_z \quad (22)$$

in order to include the Renner−Teller and spin couplings. No coordinate is kept fixed in $\hat{T}_N$. Moreover, the spin−orbit coupling is introduced perturbatively at this step by the way of $\hat{H}_{\text{SO}}$. As mentioned in ref 1, the spin−orbit operator can be approximated as

$$\hat{H}_{\text{SO}} = A_{\text{SO}} \hat{L}_z \cdot \hat{S}_z \quad (23)$$

The spin−orbit constant A_{SO} is taken to be equal to −30.23 cm^{-1}.[1]

The variational basis functions are products of one-dimensional functions

$$\Phi^{\text{vib}}_{v_i,b_i,P,\Lambda,\Sigma} = \Phi^{\text{vib}}_{v_i,b_i} \cdot \mathrm{e}^{i(P-\Lambda-\Sigma)\gamma} \quad (24)$$

where

$$\Phi^{\text{vib}}_{v_i,b_i} = \Psi^{\text{str3D}}_{v_i}(R_1, R_2, R_3) \cdot \Psi^{\text{bend3D}}_{b_i}(\theta_1, \theta_2, \phi) \quad (25)$$

$\Psi^{\text{str3D}}_{v_i}(R_1, R_2, R_3)$ is optimized at the previous stretching contraction step and

$$\Psi^{\text{bend3D}}_{b_i}(\theta_1, \theta_2, \phi) = P^{m_1}_{l_1}(\theta_1) \cdot P^{m_2}_{l_2}(\theta_2) \cdot \mathrm{e}^{i\omega\phi} \quad (26)$$

Finally, vibronic energies are obtained independently for each triplet (v_i, P, Σ).

As already emphasized by Bramley et al.,[3] the quantum numbers m_1, m_2, and ω cannot be independent in order to avoid the singularities at linearity. Indeed, the kinetic-energy operator $\hat{T}_N$ contains several terms involving $1/\sin^2\theta_1$ and $1/\sin^2\theta_2$. Since the Jacobian is proportional to $\sin\theta_1 \cdot \sin\theta_2$, after multiplication with $\hat{T}_N$, $1/\sin\theta_1$ and $1/\sin\theta_2$ terms remain and diverge for $\theta_{1,2} = 0$ or π. On the other hand, the Legrendre polynomials $P^m_l(\theta)$ contain a factor $\sin^{|m|}\theta$, and singularities occur only if $m = 0$ for the bra *and* the ket. Bramley et al. canceled this problem for nondegenerate singlet electronic states by the introduction of dependencies between the values of m_1, m_2, and ω (eqs 34 and 35 in ref 3 or eq 5 in the present work). The same relationships are used in this work to remove singularities by replacing $\hat{J}_z$ by $\hat{J}_z - \hat{L}_z - \hat{S}_z$. Then the divergences due to the following terms

$$\frac{1}{2\sin^2\theta_1}\left[\frac{1}{\mu_1 r_1^2}+\frac{1}{\mu_3 r_3^2}-\frac{2\cos\theta_1}{M_2 r_1 r_3}\right]\cdot \left[\frac{\partial^2}{\partial\phi^2}-i(\hat{J}_z-\hat{L}_z-\hat{S}_z)\frac{\partial}{\partial\phi}-\frac{(\hat{J}_z-\hat{L}_z-\hat{S}_z)^2}{4}\right] \frac{1}{2\sin^2\theta_2}\left[\frac{1}{\mu_2 r_2^2}+\frac{1}{\mu_3 r_3^2}-\frac{2\cos\theta_2}{M_3 r_2 r_3}\right]\cdot \left[\frac{\partial^2}{\partial\phi^2}+i(\hat{J}_z-\hat{L}_z-\hat{S}_z)\frac{\partial}{\partial\phi}-\frac{(\hat{J}_z-\hat{L}_z-\hat{S}_z)^2}{4}\right] \tag{27}$$

in $\hat{T}_N$ are canceled by introducing the constraints

$$m_1 = 0 \Rightarrow \omega = \frac{P-\Lambda-\Sigma}{2} \qquad m_2 = 0 \Rightarrow \omega = -\frac{P-\Lambda-\Sigma}{2} \tag{28}$$

In the previous Jacobi coordinates development,[1,2] the singularities were removed using spherical harmonics $Y_{l_i}^{m_i}(\theta_i, \phi_i)$, $i = 1, 2$. ϕ_1 and ϕ_2 are independent azimuthal angles describing the rotation of each diatomic fragment along Z^{E2} with the corresponding dependence, $e^{im_1\phi_1}\cdot e^{im_2\phi_2}$ and the restriction

$$m_1 + m_2 = P - \Lambda - \Sigma \tag{29}$$

based on the additive property of the projections along Z^{E2} of the angular momenta.

The present choice of the reference plane for the definition of BF allows linking ϕ_1 and ϕ_2 with ϕ and γ

$$\phi = \phi_2 - \phi_1 \text{ and } \gamma = (\phi_1 + \phi_2)/2 \tag{30}$$

Then the collective variation of the bending basis function with rotation angles around Z^{BF} can be decomposed in terms of ϕ_1 and ϕ_2

$$e^{i\omega\phi}\cdot e^{i(P-\Lambda-\Sigma)\gamma} = e^{i\phi_1(P-\Lambda-\Sigma/2-\omega)}\cdot e^{i\phi_2(P-\Lambda-\Sigma/2+\omega)} \tag{31}$$

The use of spherical harmonics for both diatomic fragments such as $Y_{l_1}^{m_1}(\theta_1, \phi_1)\cdot Y_{l_2}^{m_2}(\theta_2, \phi_2)$ is then equivalent to the use of $P_{l_1}^{m_1}(\theta_1)\cdot P_{l_2}^{m_2}(\theta_2)\cdot e^{i\omega\phi}\cdot e^{i(P-\Lambda-\Sigma)\gamma}$ if

$$m_1 = \left|\frac{P-\Lambda-\Sigma}{2}-\omega\right| \qquad m_2 = \left|\frac{P-\Lambda-\Sigma}{2}+\omega\right| \tag{32}$$

These equations are consistent with eq 27. To reduce the number of integral computations, we follow the same strategies as Bramley and Handy:[4] odd values of m_1 and $m_2 \geq 3$ are replaced by 1 and even values of m_1 and $m_2 \geq 4$ are replaced by 2.

The simultaneous treatment of all bending degrees of freedom makes difficult the convergence of the energies,

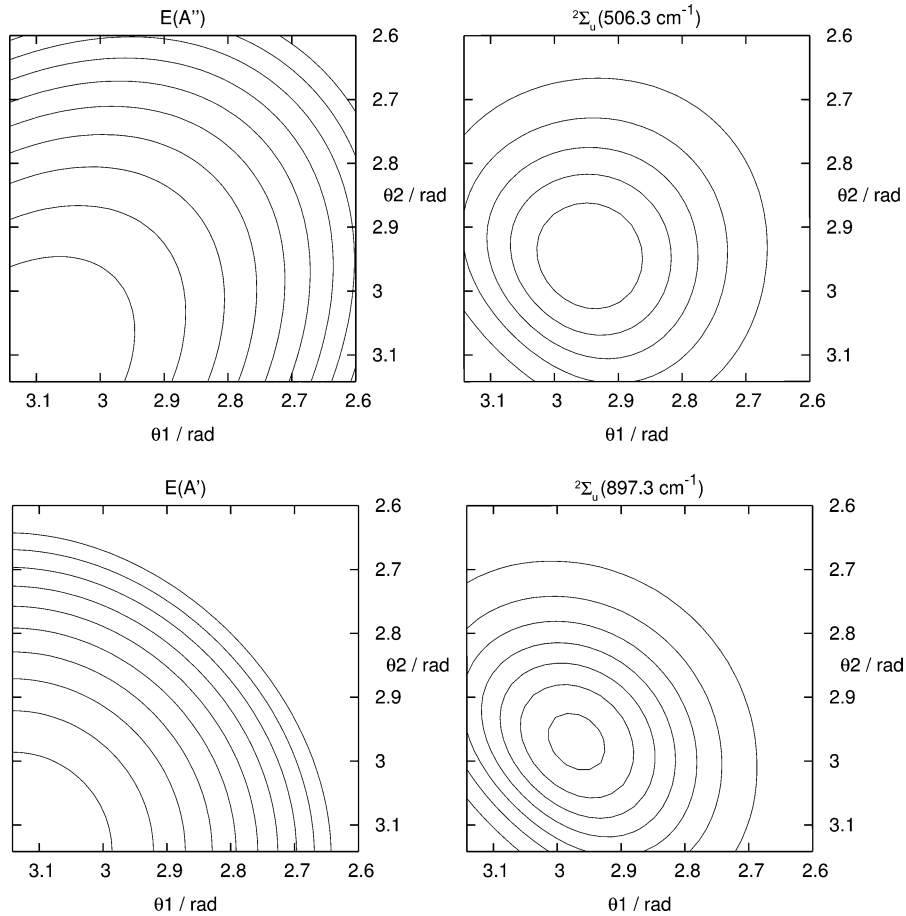

Figure 5. $HCCH^+$: Comparison between two-dimensional contour plots for the potential and both Σ states with one quantum in the trans bending mode. R_1, R_2, and R_3 are fixed at their equilibrium values, and $\phi = \pi$ (trans conformation) for all plots.

while it is not suitable to separate this ensemble of coordinates that are strongly coupled. In order to facilitate the convergence of the bending levels, factor $\exp[-10\cdot(\theta - \pi)^2]$ was introduced in the basis functions. Legende polynomials

$$P_l^m(\theta) = [\sum_{i=0}^{l-|m|} C_l^m \cos^i \theta] \cdot \sin^{|m|} \theta \quad (33)$$

are then replaced by

$$Q_l^m(\theta) = [e^{-10\cdot(\theta-\pi)^2}] \cdot [\sum_{i=0}^{l-|m|} {}^iD_l^m \cos^i \theta] \cdot \sin^{|m|} \theta \quad (34)$$

Coefficients ${}^iD_l^m$ have been determined by orthonormalization of basis functions for a given m, increasing l successively. As Legendre polynomials, these functions allow also solving the divergence problem at linearity but also are more concentrated around the linear geometries. Functions $Q_l^m(\theta)$ participate in a more general frame that is detailed in ref 24.

The basis set used in this work comprised 10 contractions for the stretches, $l_{1,\max} = l_{2,\max} = 15$ for the bending modes and $\omega_{\max} = 13/2$ for the torsion for all isotopomers. Cuts are introduced in energy at 10 000 cm^{-1} and in θ_1, θ_2 at 110°.

At this stage of our contraction scheme, the vibronic energies are overestimated for two reasons: (1) each vibronic contraction includes only one stretching function, $\Psi_{v_i}^{str3D}(R_1, R_2, R_3)$ obtained from the first contraction step and (2) the Z^{BF} axis is defined by the direction of the central stretch. In this non-Eckart frame,[25,26] the vibration−rotation separation is not optimized. It is then important to allow full mixing of the different P sets of vibronic states, even to describe accurately ideal Hund's case a.

On the other hand, this contraction step appears as being most important for assignments. At least for the lower states, it is generally possible to assign most of quanta in each vibrational mode. Then, during the final contraction step, the wave functions will be (generally) quite simple combinations of these assigned levels. Resonances will appear with several significant weights on assigned vibronic contractions.

The assignment can also be facilitated by plotting some cuts of the rovibronic wave functions Ψ or of their squared norm $|\Psi|^2$. The present contraction scheme simplifies the sum of factorized amplitudes. For instance, cuts following (θ_1, θ_2) require the sum of amplitudes for which the stretch part is the same.

Two-dimensional cuts following (θ_1, θ_2) are especially useful for analysis of Hund's case b, which are localized on one of both electronic components.[2] As an example, the shapes of $|\Psi|^2$ for the first two Σ_u states of $HCCH^+$ shown in Figure 5 follow the shapes of the PES associated with the electronic component.

For $HCCH^+$, the difficulty of defining the Renner−Teller parameter ε_5 associated with the cis bending mode, since both electronic components are very close together, was

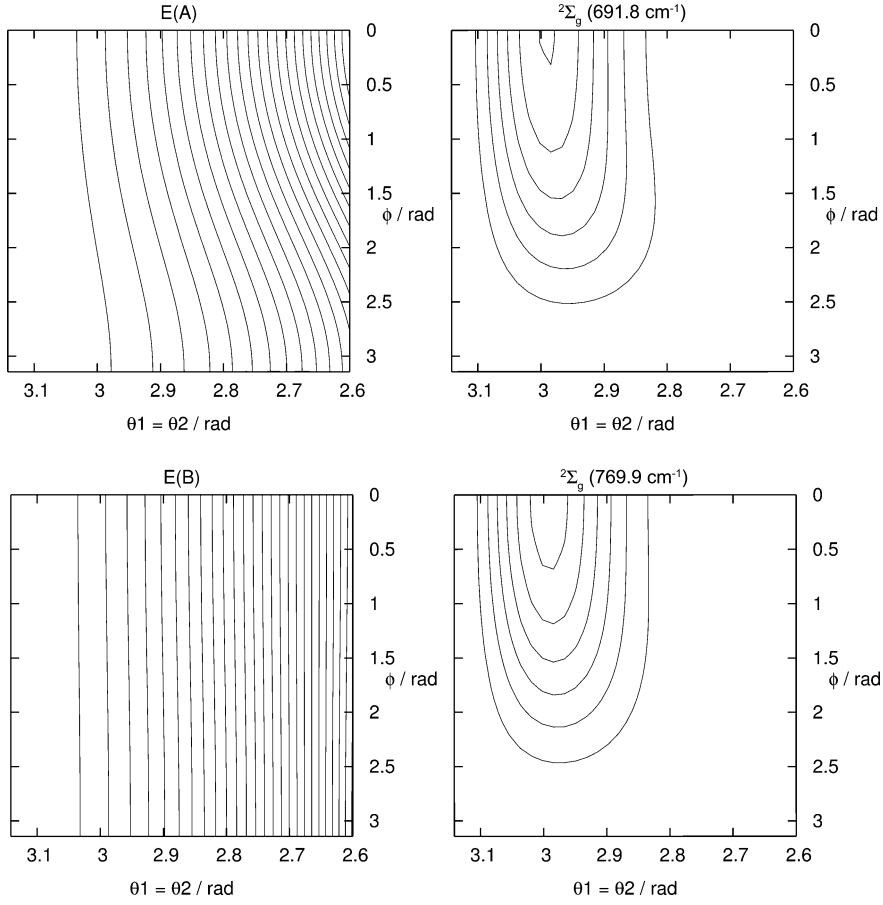

Figure 6. $HCCH^+$: Comparison between two-dimensional contour plots for the potential and both Σ states with one quantum in the cis bending mode. R_1, R_2, and R_3 are fixed at their equilibrium values.

mentioned in several experimental[7,8] and theoretical works.[2,10] Then the perturbative approach based on the harmonic approximation is not adapted to reproduce the cis bending energies. At the end, the assignment of the lower Σ state associated with one quantum in the cis bending mode can be helped by the shape of the electronic component associated with each Σ_g state. Whereas the cuts following (θ_1, θ_2) gave similar shapes for each of both $^2\Sigma_{g1/2}(\nu_5)$ states, the two-dimensional view following $[(\theta_1 = \theta_2), \phi]$ allows us to assign each Σ state with the corresponding electronic component, as shown in Figure 6.

3.3.3. Rovibronic States. In the final contraction step, all previous contractions are collected together and coupled by the complete molecular Hamiltonian $\hat{H}$. The only good quantum number is J, associated with the total angular momentum. The final basis set is now

$$\Phi^{\text{rovib}}_{v_i,b_i,J} = \Phi^{\text{vib}}_{v_i,b_i} \cdot |J, P\rangle \cdot \Phi^{\pm}_{e} \cdot |S, \Sigma\rangle \qquad (35)$$

where $\Phi^{vib}_{v_i,b_i}$ are the contracted vibronic functions of previous contraction steps. As the total kinetic-energy operator $\hat{T}_N$ adapted to the Renner−Teller and spin couplings is concerned, the full mixing between P states is allowed.

The calculations for each value of J are independent. The zero-order coefficient of the potential was removed, and all energy levels have their origin at the global minimum of the potential (at linearity in the case of $HCCH^+$). For each isotopomer, the zero-point energy is relative to the minimum of the PES and all other energies are relative to it.

The label of the final rovibronic states is based on the quantum numbers K_{space} and P, with $P = K_{\text{space}} + \Sigma$. $K_{\text{space}} = 0, \pm1, \pm2, ...$, corresponds to the Σ, Π, and Δ states, respectively. The value of P is given as the subscript, and the label u, g is the result of the combination the electronic (u) and vibrational (u, g for cis,trans bending mode) character with respect to the inversion of the rovibronic state for molecules associated with symmetry point group $D_{\infty h}$.

3.4. Preliminary Test. In order to check the largest contribution to the rovibronic energies, the $HCCH^{2+}$ dication in its fundamental state $X^3\Sigma_g^-$ is used as a testing system. The corresponding PES was obtained by Hochlaf et al.[27] at the RCCSD(T) level of theory and using the cc-pVQZ basis set. This electronic state is treated as a $^1\Sigma^+$ state in our new code, excluding the electronic angular momenta contributions, as well as in RVIB4 code based on Bramley et al.'s methodology.[28] We then neglect the spin−rotation and spin−bending couplings. Hochlaf et al. already used this PES for determination of the low-energy vibrational states at $J = 0$ and 1.[29]

The basis set used in our code was identical as the one used for $HCCH^+$, i.e., 10 contractions for the stretches, $l_{\max} = 15$ for the bending modes, and $\omega_{\max} = 13/2$ for the torsion. For RVIB4, we used 40, 70, and 70 integration points, 10, 31, and 12 initial basis functions, from which 10, 18, and 12 contracted functions are extracted for the stretches, bending modes, and torsion, respectively (see ref 4 for the details). The testing calculations are done for $J = 0$, 1, 2, and 3 and are compiled in Table 6 for rovibrational band origins up to $\sim$2600 cm^{-1} and for ν_1 and ν_3 fundamental states. The deviation between both sets of values is lower than 3 cm^{-1} for levels involving more than 3 quanta in the same bending mode and less than 1 cm^{-1} in most of cases. The rotational part of the methodology has been more accurately checked by comparing the energy difference, $\Delta E_{K,K+1}$, of the rovibrational states between $J = K_{\text{space}}$ and $J = K_{\text{space}} + 1$ calculations. As examples, $\Delta E_{K,K+1}$ values are given for some rovibronic levels in Table 7. In this way, the rovibrational part of our code has been validated.

Table 6. $HCCH^{2+}$ Rotational Band Origins (in cm^{-1}) from RVIB4 and the Present Code[a]

	$^3\Sigma_g$			$^3\Delta_g$	
$(v_4^{l_4}, v_5^{l_5})$	RVIB4	this work	$(v_4^{l_4}, v_5^{l_5})$	RVIB4	this work
$(0^0, 0^0)^-$	0.0[b]	0.0[c]			
$(0^0, 2^0)^-$	1280.2	1280.3	$(0^0, 2^2)$	1298.3	1298.4
$(2^0, 0^0)^-$	1348.2	1348.6	$(2^2, 0^0)$	1348.6	1349.6
ν_2	1517.6	1517.7			
$(0^0, 4^0)^-$	2536.7	2538.4	$(0^0, 4^2)$	2553.2	2555.3
ν_1	2737.3	2739.8			

	$^3\Sigma_u$			$^3\Delta_u$	
$(v_4^{l_4}, v_5^{l_5})$	RVIB4	this work	$(v_4^{l_4}, v_5^{l_5})$	RVIB4	this work
$(1^1, 1^1)^-$	1299.3	1299.4	$(1^1, 1^1)$	1318.4	1318.6
$(1^1, 1^1)^+$	1309.1	1309.3			
$(1^1, 3^1)^-$	2551.0	2555.2	$(1^1, 3^1)^d$	2571.0	2570.7
$(1^1, 3^1)^+$	2566.7	2571.2	$(1^1, 3^3)^d$	2586.4	2587.6
ν_3	2637.4	2637.7			

	$^3\Pi_g$			$^3\Gamma_g$	
$(v_4^{l_4}, v_5^{l_5})$	RVIB4	this work	$(v_4^{l_4}, v_5^{l_5})$	RVIB4	this work
$(1^1, 0^0)$	669.9	669.9			
$(1^1, 2^0)^d$	1933.3	1933.7			
$(1^1, 2^2)^d$	1946.3	1946.8	$(1^1, 2^2)$	1967.8	1968.5
$(3^1, 0^0)$	2035.4	2037.6	$(3^3, 0^0)$	2036.3	2037.8
$\nu_2(1^1, 0^0)$	2172.2	2172.8			

	$^3\Pi_u$			$^3\Gamma_u$	
$(v_4^{l_4}, v_5^{l_5})$	RVIB4	this work	$(v_4^{l_4}, v_5^{l_5})$	RVIB4	this work
$(0^0, 1^1)$	648.3	648.3			
$(0^0, 3^1)$	1916.3	1916.6	$(0^0, 3^3)$	1950.4	1949.9
$(2^0, 1^1)^d$	1968.1	1968.8			
$(2^2, 1^1)^d$	1989.8	1991.1	$(2^2, 1^1)$	1998.6	1998.7
$\nu_2(0^0, 1^1)$	2165.3	2165.3			

[a] ν_4, ν_5 correspond to the trans and cis bending modes, respectively. [b] ZPE: 4905.6 cm^{-1}. [c] ZPE: 4905.8 cm^{-1}. [d] Tentative assignment.

Table 7. $HCCH^{2+}$ $\Delta E_{K,K+1}$ (in cm^{-1}) from RVIB4 and the Present Code[a]

	$\Delta E_{K,K+1}$	
state $(v_4^{l_4}, v_5^{l_5})$	RVIB4	this work
$^3\Sigma_g^-(0^0, 0^0)^-$	1.9483	1.9486
$^3\Sigma_u^-(1^1, 1^1)^-$	1.9529	1.9534
$^3\Pi_g(1^1, 2^0)$	3.9571	3.9533
$^3\Pi_u(0^0, 1^1)$	3.9168	3.8992
$^3\Delta_g(2^2, 0^0)$	6.9288	5.8456

[a] ν_4, ν_5 correspond to the trans and cis bending modes, respectively.

Table 8. $HCCH^+$ Rotational Band origins (in cm^{-1})

state	assignment	previous work[2]	Tang[7]	Yang[8] [b]	this work
$^2\Pi_{u3/2}$	0	0.0	0.0	0.0	0.0[c]
$^2\Pi_{u1/2}$		28.5	30.8	29.8	28.5
$^2\Sigma_{u1/2}$	ν_4	496.2	502.7	499.5	506.3
$^2\Delta_{u5/2}$		658.6	666.4	672.9	665.0
$^2\Delta_{u3/2}$		685.8	695.8	701.4	692.3
$^2\Sigma_{u1/2}$		902.3	912.6	909.9	897.3
$^2\Sigma_{g1/2}$	ν_5	685.4	697.5	694.9	691.8
$^2\Delta_{g5/2}$		718.9	715.1	713.4	718.7
$^2\Delta_{g3/2}$		747.5	746.0	743.0	747.4
$^2\Sigma_{g1/2}$		776.2	746.6	738.2	769.9
$^2\Pi_u$	$2\nu_4$	1090.7	1109.4	1108.3	1105.1
$^2\Phi_{u7/2}$		1313.5	1327.0	1316.0	1323.2
$^2\Phi_{u5/2}$		1338.8	1354.3	1342.7	1348.8
$^2\Pi_u$		1685.5		1683.5	1682.3
$^2\Pi_g$	$\nu_4 + \nu_5$	1214.9	1210.8[a]	1210.2	1236.8
$^2\Pi_{g3/2}$		1365.6	1361.6	1373.1	1373.2
$^2\Pi_{g1/2}$		1392.9	1390.7	1401.6	1403.8
$^2\Phi_{g7/2}$		1384.5	1384.1	1370.4	1392.0
$^2\Phi_{g5/2}$		1411.9	1414.2	1398.9	1420.0
$^2\Pi_g$		1613.7	1616.8[a]	1620.6	1608.5
$^2\Pi_u$	$2\nu_5$	1392.5	1393.5	1404.8	1399.3
$^2\Phi_{u7/2}$		1423.8	1432.7	1410.7	1439.3
$^2\Phi_{u5/2}$		1452.6	1462.8	1440.5	1468.1
$^2\Pi_u$		1496.4	1459.0[a]	1451.2	1487.4
$^2\Pi_{u3/2}$	ν_2	1819.0		1817.5	1818.9
$^2\Pi_{u1/2}$		1847.5			1846.8
$^2\Pi_{g3/2}$	ν_3	3151.9[d]			3134.3
$^2\Pi_{u3/2}$	ν_1	3236.4[d]			3221.8

[a] Undetermined A_{SO}. [b] Data from Table 7 of ref 8. [c] ZPE: 5572.9 cm^{-1}. [d] Stretching contractions without coupling with the other degrees of freedom.

Table 9. $DCCD^+$ Rotational Band origins (in cm^{-1})

state	assignment	Perić[11] [a]	this work
$^2\Pi_{u3/2}$	0	0	0.0[b]
$^2\Pi_{u1/2}$		0 + 28.46	28.8
$^2\Sigma_{u1/2}$	ν_4	418 − 0.56	420.9
$^2\Delta_{u5/2}$		573 − 27.04/2	552.9
$^2\Delta_{u3/2}$		573 + 27.04/2	580.2
$^2\Sigma_{u1/2}$		782 + 0.54	751.7
$^2\Sigma_{g1/2}$	ν_5	539 − 8.97	511.7
$^2\Delta_{g5/2}$		546 − 28.46/2	530.0
$^2\Delta_{g3/2}$		546 + 28.46/2	558.9
$^2\Sigma_{g1/2}$		553 + 8.95	574.4
$^2\Pi_u$	$2\nu_4$	923	917.6
$^2\Phi_{u7/2}$		1077 − 28.45/2	1060.9
$^2\Phi_{u5/2}$		1077 + 28.45/2	1090.0
$^2\Pi_u$		1435	1397.1
$^2\Pi_g$	$\nu_4 + \nu_5$	950	959.2
$^2\Pi_{g3/2}$		1103 − 27.04/2	1078.0
$^2\Pi_{g1/2}$		1103 + 27.04/2	1105.8
$^2\Phi_{g7/2}$		1089 − 27.04/2	1087.1
$^2\Phi_{g5/2}$		1089 + 27.04/2	1114.8
$^2\Pi_g$		1314	1274.4
$^2\Pi_u$	$2\nu_5$	1068	1034.4
$^2\Phi_{u7/2}$		1115 − 25.15/2	1098.0
$^2\Phi_{u5/2}$		1115 + 25.15/2	1123.7
$^2\Pi_u$		1087	1104.7
$^2\Pi_{u3/2}$	ν_2		1637.6
$^2\Pi_{u1/2}$			1665.9
$^2\Pi_{g3/2}$	ν_3		2326.4 − 2327.3[c]
$^2\Pi_{u3/2}$	ν_1		2571.4

[a] $E_{niv} = E_{rovib} + E_{SO}$; the effect of the spin−orbit coupling is added to the rovibronic energies. Except for states $^2\Pi_{u3/2}$ and $^2\Pi_{u1/2}$, all values of E have been shifted by 14 cm^{-1}. [b] ZPE: 4405.5 cm^{-1}. [c] Resonance with a Hund's case b state. Both states energies are given.

4. Results

We present here the rovibronic levels computed for $HCCH^+$, $DCCH^+$, and $DCCD^+$ up to two quanta in the bending modes.

4.1. Rotational Band Origins for the Symmetrical $HCCH^+$ and $DCCD^+$. The final rovibronic contracted state energy levels corresponding to rotational band origins for $HCCH^+$ and $DCCD^+$ are displayed in Tables 8 and 9. They are both associated with the $D_{\infty h}$ symmetry point group, and the same assignment is adopted.

In Table 8, the rovibronic energies of $HCCH^+$ coming from valence coordinates development roughly agree with photoelectron spectroscopy data[7,8] and the ones computed previously by Jacobi coordinates treatment. A value of P is given only when it corresponds almost to a good quantum number: (i) for Σ states $P = 1/2$, (ii) in degenerate Hund's case a, for which we obtain a separation between both components $P = K_{space} \pm 1/2$. On the other hand, for degenerate Hund's case b, spin−rotation couplings play a crucial role in the wave functions, so that both spin components are strongly mixed together except for the lowest value of J.

For both symmetrical isotopomers, the classification of Hund's cases a and b is very standard for systems having a weak spin−orbit constant: Hund's case b go by pairs, with one state on the lower electronic component and the other one on the upper component. Single states are Hund's case a, delocalized on both electronic components. It is worth noting that Σ states are generally Hund's case b, and they always are if the spin−orbit constant is negligible.

For $DCCD^+$, the present results are in good agreement with the values determined by Perić et al.,[11] who separated the effects of the spin−orbit coupling as emphasized in Table 9. Except for the fundamental states, all rovibronic energies, without the effect of the spin−orbit coupling, are shifted by 14 cm^{-1} in order to facilitate the comparison. As in $HCCH^+$ (see Figure 8 in ref 2), the non-negligible spin−orbit coupling between the first two Σ states with one quantum in the cis bending mode (almost ± 8.97 cm^{-1} for Perić et al., while we find ± 5.6 cm^{-1}) is the signature of an intermediate nature between Hund's cases a and b due to the weak Renner−Teller splitting between both electronic components in the cis conformation (see section 3.2). Indeed, factorization of the total wave function by one of each electronic component involves a cancellation of the spin−orbit coupling, while factorization by one of each eigenfunction of $\hat{L}_z$, giving rise to a maximum contribution of the spin−orbit coupling, corresponds to a complete delocalization on both electronic components. Renner−Teller effect and spin−orbit couplings are then directly in competition for the Σ states. Moreover, we notice that the rotational excited states of Π states at 1105.8 and 1104.7 cm^{-1} are strongly mixed.

We also give the first excitation of the stretching modes. For $HCCH^+$, $\nu_3 = 3134.3$ cm^{-1} and $\nu_1 = 3221.8$ cm^{-1}. These values are in remarkable agreement with the best experimental results at 3135.9813 and 3226.6 cm^{-1}, respectively, from refs 30 and 31. From photoelectron spectroscopy, Reutt et al. deduced $\nu_2 = 1829.0(2.5), 1651(4)$ cm^{-1} agreeing within 10, 14 cm^{-1} with the present computed energies for

Table 10. HCCD$^+$ Rovibronic Levels (in cm^{-1})[a]

state	assignment	Perić[12] [b]	this work
$^2\Pi_{3/2}$	0	14	0.0[c]
$^2\Pi_{1/2}$		14	28.7
$^2\Sigma_{1/2}$	ν_5	438	442.3
$^2\Delta_{5/2}$		561	543.9
$^2\Delta_{3/2}$		561	571.9
$^2\Sigma_{1/2}$		621	582.3
$^2\Sigma_{1/2}$	ν_4	656	692.6
$^2\Delta_{5/2}$		711	690.5
$^2\Delta_{3/2}$		711	718.7
$^2\Sigma_{1/2}$		889	847.0
$^2\Pi$	$2\nu_5$	946	953.4
$^2\Phi_{7/2}$		1102	1088.3
$^2\Phi_{5/2}$		1102	1115.5
$^2\Pi$	resonance	1114	1099.9
$^2\Pi_{3/2}$	$(\nu_4 + \nu_5)/(2\nu_5)$	1183	1140.1
$^2\Pi_{1/2}$		1183	1160.5
$^2\Phi_{7/2}$	$\nu_4 + \nu_5$	1250	1229.7
$^2\Phi_{5/2}$		1250	1256.8
$^2\Pi$		1264	1261.0
$^2\Pi_{(1/2)}$		1466	1434.8
$^2\Pi_{(3/2)}$		1466	1441.8
$^2\Pi_{3/2}$	$2\nu_4$	1341	1347.3
$^2\Pi_{1/2}$		1341	1368.0
$^2\Phi_{7/2}$		1404	1385.8
$^2\Phi_{5/2}$		1404	1413.7
$^2\Pi$		1658	1596.1
$^2\Pi_{3/2}$	ν_3		1717.2
$^2\Pi_{1/2}$			1745.0
$^2\Pi_{3/2}$	ν_2		2454.8
$^2\Pi_{3/2}$	ν_1		3184.0

[a] ν_4, ν_5 correspond to the bending of the $\hat{CCH}$, $\hat{DCC}$ angles, respectively. [b] $E_{niv} = E_{rovib}$; the effect of the spin−orbit coupling has not been taken into account in ref 12. All values of E have been shifted by 14 cm^{-1}. [c] ZPE: 4990.6 cm^{-1}.

HCCH$^+$, DCCD$^+$, respectively.[9] For DCCD$^+$, they obtained $\nu_1 = 2572(14)$ cm^{-1}, which coincides with the present calculated value of 2571.4 cm^{-1}. They also extracted, from experimental data, a Renner−Teller multiplet origin for the trans bending mode ν_4 at 702(12) cm^{-1} for DCCD$^+$. From our experience, the $^2\Delta_{u5/2}$ is the closest rovibronic level to the perturbative Renner−Teller multiplet origin. We computed $^2\Delta_{u5/2}$ at 552.9 cm^{-1} quite far from this extracted experimental value. We cannot make a conclusion about the accuracy of either the experimental measurement or the theoretical calculations since, for Renner−Teller systems including spin−orbit coupling, the extraction of spectroscopic constants from observed spectra is sometimes quite problematic.[8,10] In particular, in more than three atom molecules, the number of interdependent perturbative parameters can make the accurate determination of each one difficult.

4.2. Rotational Band Origins for the Nonsymmetrical DCCH$^+$. For DCCH$^+$, the inversion symmetry disappears and the assignment of the bending levels raises further difficulties. Indeed, both bending modes belong to the same representation Π and new resonances are allowed. The ν_4 and ν_5 modes are mostly associated with the $\widehat{CCH}$, $\widehat{DCC}$ bending angles, respectively. As in Table 8, a value of P is given only when it corresponds almost to a good quantum number.

The final rovibronic state energy levels corresponding to rotational band origins for DCCH$^+$ are displayed in Table 10, in comparison with the results obtained by Perić et al. without spin−orbit coupling.[12] All their energies are shifted by 14 cm^{-1} in order to have a common reference. Most of these results are in good agreement. The main significant divergence is due to a resonance that we found between ν_4

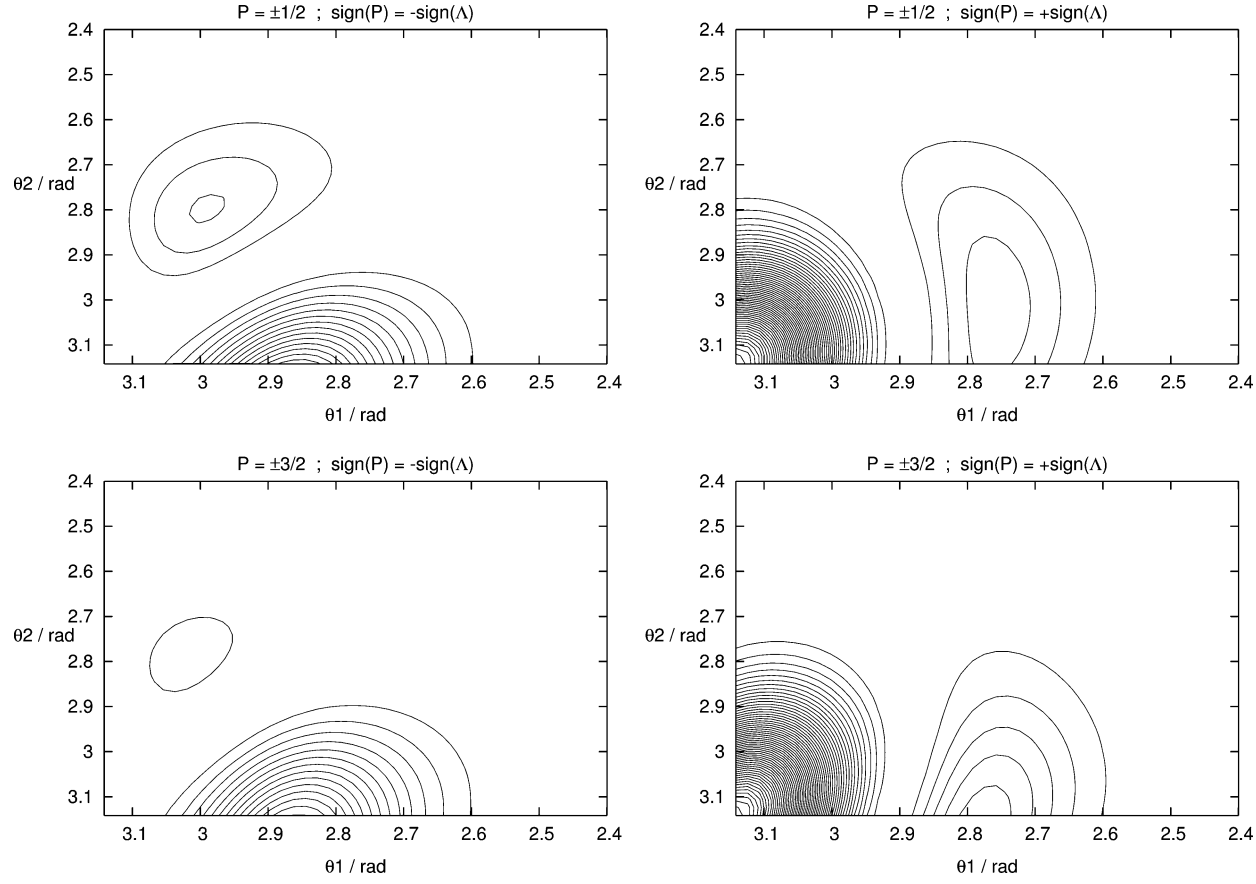

Figure 7. DCCH$^+$: Contractions which contribute mainly to the states belonging to the resonance $[(\nu_4 + \nu_5) + (2\nu_5)]$.

and ν_5. Indeed, the assignments of both Σ states at 582.3 and 692.6 cm^{-1} are approximative, while they are both coupled together. This leads to a minimization of the lower state energy and to an augmentation of the upper state energy. This fact explains the inversion between the energies of the Σ state at 692.6 cm^{-1} and of the Δ state at 690.5 cm^{-1}.

With two quanta in bending modes, the structure in Hund's cases a and b of Π states is not well conserved. Even an "anti-Hund's case a" contribution is observed in both states assigned Π at 1434.8 and 1441.8 cm^{-1}, for which component $|P| = 1/2$ possesses a lower energy than component $|P| = 3/2$. Moreover, the spin−orbit splitting for Hund's case a is reduced to around 20 cm^{-1} instead of 27 cm^{-1} in $HCCH^+$. On the other hand, a standard repartition such as the one obtained for both symmetrical isotopomers would lead to only one Hund's case a pair of states, i.e., $(^2\Pi_{g3/2}/^2\Pi_{g1/2})$, instead of two $(^2\Pi_{3/2}/^2\Pi_{1/2})$ pairs at energies (1140.1/1160.5) and (1347.3/1368.0) cm^{-1}. However, the averaged Hund's cases a and b are conserved.

The resonance between $(\nu_4 + \nu_5)$ and $2\nu_5$ can be visualized by plotting each contribution $\pm \Lambda$ independently. As this resonance couples different values of Λ, the distorted wave function shapes usually obtained in the case of Fermi resonances as in ref 32 are avoided. In Figure 7, two-dimensional contours of the contractions which contribute mainly to the Hund's case b $^2\Pi$ state obtained at 1099.9 cm^{-1} are plotted. The rotational band origin, for which $|P| = 1/2$, is only concerned in the first two plots, while all states for which $J \geq 1/2$ are combinations of the four plots. Perić et al. also expect a significant contribution of $2\nu_4$ for this state. This last point could explain, for both left-hand side figures, the less important part of the wave function following the θ_2 axis, since both $(\nu_4 + \nu_5)$ and $2\nu_4$ contractions contribute to the wave functions with $sign(P) = -sign(\Lambda)$, but they are in phase opposition. However the complete decomposition of the total spin-rovibronic functions is more complicated to analyze, since the contributions corresponding to $sign(P) = -sign(\Lambda)$ do not have a significant weight at linearity, in contrast with $2\nu_4$. For comparison, Figure 8 shows the main contributions of the more standard Hund's case b $^2\Pi$ state obtained at 1261.0 cm^{-1} assigned to $(\nu_4 + \nu_5)$.

In conclusion, for nonsymmetrical systems, the diminution of the irreducible representations number entails much more resonance phenomena, even at low energy. In addition, because Renner−Teller systems involve two times more states for a given number of quanta in vibrational modes and because the hierarchy between the corresponding coupling and the spin−orbit one is not always sharply contrasted, it is often impossible to achieve a standard analysis in terms of assignments and Hund's cases as in perturbative approaches. Most of them are indicative.

4.3. Rotational Structures. As already discussed in previous articles,[1,2] the rotational structures attempted for Hund's cases a and b states are very different. For Hund's case a states, two independent rotational structures can be defined from both spin components $P = K_{space} \pm 1/2$. For Hund's case b states, P is not a good quantum number and the spin−rotation coupling has a crucial role as well as spin-

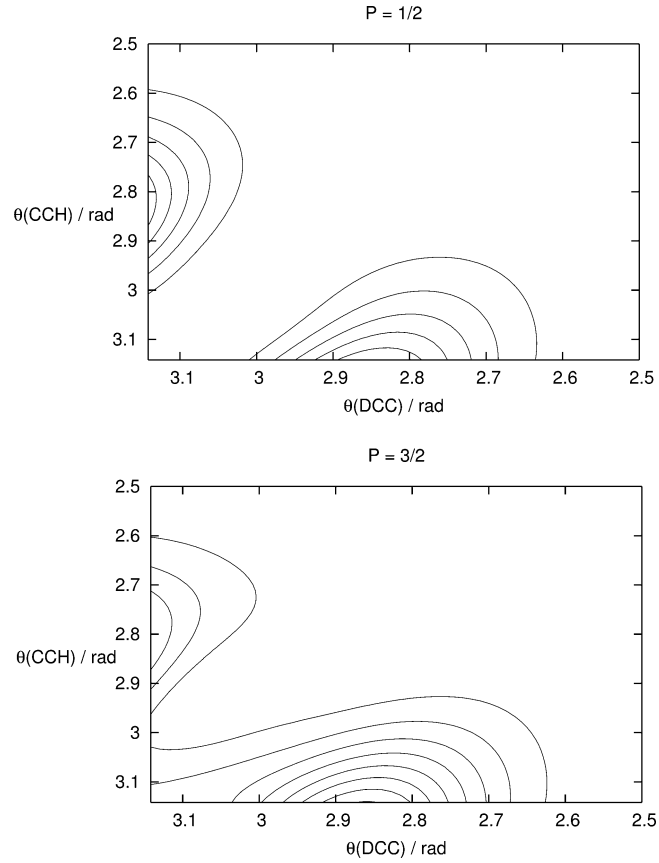

Figure 8. $DCCH^+$: Contractions which contribute mainly to the Hund's case b $^2\Pi$ state at 1261.0 cm^{-1} assigned to $(\nu_4 + \nu_5)$.

bending couplings. However, spin−rotation couplings also have an effect on the rotational structure of Hund's case a. Indeed, small couplings between both spin components induce a mix between them. Even whether it concerns only few 10^{-2}%, it is sufficient to affect the effective rotational constants B_{eff} (defined as the energy difference of the $J = P$ and $J = P + 1$ states for a given rotational band origin divided by $(P + 1)(P + 2) - P(P + 1)$). For instance, in the case of the $^2\Pi$ fundamental state with no quantum in vibrational modes: $B_{eff(P=3/2)} = 1.064$ cm^{-1} and $B_{eff(P=1/2)} = 1.139$ cm^{-1} for $HCCH^+$, $B_{eff(P=3/2)} = 0.904$ cm^{-1} and $B_{eff(P=1/2)} = 0.958$ cm^{-1} for $DCCH^+$, and $B_{eff(P=3/2)} = 0.777$ cm^{-1} and $B_{eff(P=1/2)} = 0.818$ cm^{-1} for $DCCD^+$. For Hund's case b states, the rotational structures of the first three energy states are displayed in Table 11. In the case of $HCCH^+$, the present values are compared with the experimental work made by Yang et al.[8] and with our previous work. The global agreement makes us confident with our results for $DCCH^+$ and $DCCD^+$, which are predictive.

The most common rotational structures for Σ Hund's case b states is as follows: a band origin given by the $(J = 1/2, F1)$ component; a succession of couple of states very close in energy, corresponding to $(J, F2)$ and $(J + 1, F1)$. Both states cannot be coupled without an external field, because J is still a good quantum number. Their energy order is often difficult to define and can vary under even very small couplings of any kind with other states.

Table 11. Rotational Structures (in cm^{-1}) from a Nondegenerate Σ and Two Degenerate Π Vibronic States (all Hund's case b states)[a]

lowest energy $^2\Sigma$ state						
$HCCH^+$					$DCCH^+$	$DCCD^+$
band origin-ZPE: Yang 499.5; previous work 496.2; this work 506.3					band origin-ZPE: this work 442.3	band origin-ZPE: this work 420.9
J	F	Yang	previous work	this work	this work	this work
1/2	F1	0.0	0.0	0.0	0.0	0.0
1/2	F2		2.2	2.2	1.8	1.6
3/2	F1	2.3	2.1	2.2	1.9	1.6
3/2	F2	6.7	6.7	6.6	5.6	4.8
5/2	F1		6.5	6.6	5.6	4.8
5/2	F2	13.4	13.3	13.2	11.2	9.6
7/2	F1		13.1	13.2	11.2	9.6
7/2	F2		22.1	22.0	18.6	15.9

lowest energy $^2\Pi$ state with two quanta in bending modes						
$HCCH^+$					$DCCH^+$	$DCCD^+$
band origin-ZPE: Yang 1108.3; previous work 1090.7; this work 1105.1					band origin-ZPE: this work 953.4	band origin-ZPE: this work 917.6
J	F	Yang	prev. work	this work	this work	this work
1/2	F1		1.9	1.8	0.9	1.8
3/2	F1	0.0	0.0	0.0	0.0	0.0
3/2	F2		5.9	5.9	4.4	4.7
5/2	F1	4.6	4.6	4.6	3.9	3.4
5/2	F2		12.3	12.3	9.9	9.3
7/2	F1	11.3	11.3	11.4	9.6	8.4
7/2	F2	20.9	21.0	21.0	17.4	15.7

second $^2\Pi$ state with two quanta in bending modes						
$HCCH^+$					$DCCH^+$	$DCCD^+$
($J = 1/2$, F1)-ZPE: Yang 1210.2; previous work 1214.9; this work 1237.4					band origin-ZPE: this work 1099.9	band origin-ZPE: this work 959.2
J	F	Yang	previous work	this work	this work	this work
1/2	F1	0.0	0.0	0.0	0.0	0.4
3/2	F1		−0.8	−0.6	1.7	0.0
3/2	F2	4.2	4.2	4.2	5.2	3.5
5/2	F1	4.6	3.7	3.9	5.4	3.3
5/2	F2		10.8	10.6	10.9	8.2
7/2	F1		10.4	10.5	11.1	8.1
7/2	F2		19.6	19.7	18.4	14.6

[a] Yang and previous work are associated with refs 8 and 2, respectively.

The most common rotational structures for degenerate Π Hund's case b states are as follows: a band origin given by the $(J = 3/2, F1)$ component, followed by $(J = 1/2, F1)$. The energy difference between both is variable and depends on small spin−orbit couplings, spin−rotation, spin−bending, and a succession of couple of states very close in energy, corresponding to $(J, F2)$ and $(J + 1, F1)$, with the same remark as for Σ states.

The only case for which a deviation from this general scheme is observed concerns the rotational structure from the Π state of $DCCH^+$ obtained at 1099.9 cm^{-1}. We have already seen that this state belongs to a complicated resonance between several assignments with two quanta in the bending modes.

Actually, the rotational structures shown in Table 11 are simplified. Indeed, in the molecular symmetry groups $D_{\infty h}(MS)$ and $C_{\infty v}(MS)$, all irreducible representations are nondegenerate, in contrast with the corresponding symmetry point groups. The notations (J, F) should correspond to degenerate states, except for rotational structures from Σ states; however, the corresponding degeneracy is slightly raised. Then numbers in Table 11 are given with only one digit since inside each pair of states energies are very close together at low values of *J* but can be spaced by few times 0.1 cm^{-1} for $J \geq 7/2$. These effects should be pointed out for higher values of *J* and vary a lot particularly because the couplings with Σ states affect both components of a given (J, F) assignment independently.

5. Conclusions

In the present work, a new variational methodology for treatment of the Renner−Teller effect in tetra-atomic molecules is developed in valence coordinates. The kinetic-energy operator of Bramley et al.[3,4] for any sequentially bonded four-atom molecule, A−B−C−D, in a singlet nondegenerate electronic state has been adapted to the Renner−Teller and spin couplings by modifying the expression of the rotational angular momentum. The total Schrödinger equation is solved by diagonalizing the Hamiltonian matrix in a three-step contraction scheme. The present methodology has been checked by comparing

rovibrational energies of the $X^3\Sigma_g^-$ electronic ground state of $HCCH^{2+}$ obtained from the present code, without taking into account the orbital and spin electronic angular momenta, and a variational code based on Bramley et al. works. Both sets of results are in remarkably good agreement for the rovibrational band origins as well as for rotational structures.

The main advantage of this new theoretical development is the possibility of studying different isotopomers using the same potential-energy surfaces. This procedure has been tested on $HCCH^+$ and its deuterated derivatives $DCCD^+$ and $DCCH^+$. The calculated rovibronic band origins have been compared with previous data deduced from Jacobi coordinates methodology,[1,2] dimensionality reduced variational treatment,[11,12] and photoelectron spectra[7−9] with an overall good agreement.

Finally, this new methodology will permit the variational treatment of systems for which Jacobi coordinates involve much too high crossing terms in the PESs such as HCCS or HCCO where at least one external atom possesses a comparable or higher weight than the central atoms directly linked to it.

Acknowledgment. This work was partially supported by the French "Centre National de la Recherche Scientifique" (CNRS). The authors thank Prof. M. Hochlaf for discussions on the $HCCH^{2+}$ PES.

References

(1) Jutier, L.; Léonard, C.; Gatti, F. *J. Chem. Phys.* **2009**, *130*, 134301.

(2) Jutier, L.; Léonard, C.; Gatti, F. *J. Chem. Phys.* **2009**, *130*, 134302.

(3) Bramley, M. J.; Green, W. H.; Handy, N. C. *Mol. Phys.* **1991**, *73*, 1183.

(4) Bramley, M. J.; Handy, N. C. *J. Chem. Phys.* **1993**, *98*, 1378.

(5) Carter, S.; Handy, N. C.; Rosmus, P.; Chambaud, G. *Mol. Phys.* **1990**, *71*, 605.

(6) Carter, S.; Handy, N. C.; Puzzarini, C.; Tarroni, R.; Palmieri, P. *Mol. Phys.* **2000**, *98*, 1697.

(7) Tang, S.-J.; Chou, Y.-C.; Lin, J. J.-M.; Hsu, Y.-C. *J. Chem. Phys.* **2006**, *125*, 133201.

(8) Yang, J.; Mo, X. *J. Phys. Chem. A* **2006**, *110*, 11001.

(9) Reutt, J. E.; Wang, L. S.; Pollard, J. E.; Trevor, D. J.; Lee, Y. T.; Shirley, D. *J. Chem. Phys.* **1985**, *84*, 3022.

(10) Perić, M.; Thümmel, H.; Marian, C. M.; Peyerimhoff, S. D. *J. Chem. Phys.* **1995**, *102*, 7142.

(11) Perić, M.; Radić-Perić, J. *J. Chem. Phys. Lett.* **1998**, *290*, 443.

(12) Perić, M.; Ostojić, B.; Radić-Perić, J. *J. Chem. Phys.* **1999**, *110*, 4783.

(13) Žabka, J.; Dolejšek, Z.; Hrušák, J.; Herman, Z. *Int. J. Mass Spectrom.* **1999**, *185/186/187*, 95.

(14) Bockelee-Morvan, D.; Gautier, D.; Lis, D.; Young, K.; Keene, J.; Phillips, T.; Owen, T.; Crovisier, J.; Goldsmith, P.; Bergin, E.; Despois, D.; Wootten, A. *Icarus* **1999**, *133*, 147.

(15) Zare, R. N. *Angular Momentum*; Wiley: New York, 1988.

(16) Gatti, F.; Nauts, A. *Chem. Phys.* **2003**, *295*, 167.

(17) Klein, O. Z. *Phys.* **1929**, *58*, 730.

(18) Brown, J. M.; Howard, B. J. *Mol. Phys.* **1976**, *31*, 1517.

(19) Knowles, P. J.; Hampel, C.; Werner, H.-J. *J. Chem. Phys.* **1993**, *99*, 5219.

(20) Knowles, P. J.; Hampel, C.; Werner, H.-J. *J. Chem. Phys.* **2000**, *112*, 3106.

(21) Watts, J. D.; Gauss, J.; Bartlett, R. J. *J. Chem. Phys.* **1993**, *98*, 8718.

(22) Dunning, J., T. H. *J. Chem. Phys.* **1989**, *90*, 1007.

(23) Werner, H.-J.; Knowles, P. J.; Lindh, R.; Manby, F. R.; Schütz, M. MOLPRO: a package of ab initio programs, version 2008.1; http://www.molpro.net.

(24) Jutier, L. Manuscript in preparation.

(25) Eckart, C. *Phys. Rev.* **1935**, *47*, 552.

(26) Sayvetz, A. *J. Chem. Phys.* **1939**, *7*, 383.

(27) Hochlaf, M. Private communication.

(28) RVIB4 is a tetraatomic rovibrational variational code, see: Carter, S.; Handy, N. *J. Mol. Spectrosc.* **1998**, *192*, 263. *J. Phys. Chem. A*, **1998**, *102*, 6325. *Mol. Phys.*, **1997**, *90*, 729. *J. Mol. Spectrosc.*, **1993**, *157*, 301, and references therein.

(29) Hochlaf, M.; Palaudoux, J.; Ben Houria, A. *Recent Res. Dev. Chem. Phys.* **2004**, *5*, 403.

(30) Jagod, M.-F.; Rösslein, M.; Gabrys, C. M.; Rehfuss, B. D.; Scappini, F.; Crofton, M. W.; Oka, T. *J. Chem. Phys.* **1992**, *97*, 7111.

(31) Forney, D.; Jacox, M. E.; Thompson, W. E. *J. Mol. Spectrosc.* **1992**, *153*, 680.

(32) Stimson, S.; Evans, M.; Ng, C.; Hsu, C.-W.; Heimann, P.; Destandau, C.; Chambaud, G.; Rosmus, P. *J. Chem. Phys.* **1998**, *108*, 6205.

CT100071D